Accumulation of Free Oligosaccharides and Tissue Damage in Cytosolic α-Mannosidase (Man2c1)-deficient Mice

Silvia Paciotti[‡], Emanuele Persichetti[‡], Katharina Klein[§], Anna Tasegian[‡], Sandrine Duvet[¶], Dieter Hartmann[∥], Volkmar Gieselmann[§], and Tommaso Beccari[‡1]

From the [‡]Dipartimento di Scienze Farmaceutiche, University of Perugia, Perugia 06126, Italy, the [§]Institut für Biochemie und Molekularbiologie, Rheinische Friedrich-Wilhelms-Universität Bonn, 53115 Bonn, Germany, the [¶]Unité de Glycobiologie Structurale et Fonctionnelle, Université des Sciences et Technologies de Lille, 59655 Villeneuve d'Ascq, France, and the [∥]Institute of Anatomy, University of Bonn, Nussallee 10, 53115 Bonn, Germany

Background: Cytosolic α-mannosidase (Man2c1) is involved in the catabolism of free oligosaccharides (fOS).
Results: Man2c1-deficient mice accumulate fOS in tissues and show biochemical and histological alterations in the CNS, liver, and intestine.
Conclusion: Man2c1 plays an essential role in the catabolism of fOS.
Significance: Man2c1-deficient mice could be a useful tool to examine the biological significance of Man2c1.

Free $Man_{7-9}GlcNAc_2$ is released during the biosynthesis pathway of *N*-linked glycans or from misfolded glycoproteins during the endoplasmic reticulum-associated degradation process and are reduced to $Man_5GlcNAc$ in the cytosol. In this form, free oligosaccharides can be transferred into the lysosomes to be degraded completely. α-Mannosidase (MAN2C1) is the enzyme responsible for the partial demannosylation occurring in the cytosol. It has been demonstrated that the inhibition of MAN2C1 expression induces accumulation of $Man_{8-9}GlcNAc$ oligosaccharides and apoptosis *in vitro*. We investigated the consequences caused by the lack of cytosolic α-mannosidase activity *in vivo* by the generation of *Man2c1*-deficient mice. Increased amounts of $Man_{8-9}GlcNAc$ oligosaccharides were recognized in all analyzed KO tissues. Histological analysis of the CNS revealed neuronal and glial degeneration with formation of multiple vacuoles in deep neocortical layers and major telencephalic white matter tracts. Enterocytes of the small intestine accumulate mannose-containing saccharides and glycogen particles in their apical cytoplasm as well as large clear vacuoles in retronuclear position. Liver tissue is characterized by groups of hepatocytes with increased content of mannosyl compounds and glycogen, some of them undergoing degeneration by hydropic swelling. In addition, lectin screening showed the presence of mannose-containing saccharides in the epithelium of proximal kidney tubules, whereas scattered glomeruli appeared collapsed or featured signs of fibrosis along Bowman's capsule. Except for a moderate enrichment of mannosyl compounds and glycogen, heterozygous mice were normal, arguing against possible toxic effects of truncated Man2c1. These findings confirm the key role played by Man2c1 in the catabolism of free oligosaccharides.

N-linked glycoproteins of mammalian cells are synthesized in the endoplasmic reticulum (ER)[2] and complete their matu-ration in the Golgi complex. Before their transport to the Golgi apparatus, newly synthesized glycoproteins are submitted to quality control, ensuring that only correctly folded glyco-proteins leave the ER. Misfolded glycoproteins bearing $Man_{7-9}GlcNAc_2$ oligosaccharides are retrotranslocated to the cytosol to be degraded via the ER-associated degradation (ERAD) process (1, 2). The ERAD pathway begins with the release of the oligosaccharides by a peptide *N*-glycanase activity in the cytosol (3). The polyubiquitinated peptide backbone is degraded in the proteasome complex (4). The remaining free oligosaccharides (fOS) bear two GlcNAc residues at their reducing ends (called fOSGN2). They are subsequently trimmed by the β-endo-*N*-acetylglucosaminidase (ENGase), resulting in the formation of oligosaccharides possessing a sin-gle GlcNAc residue at their reducing ends (called fOSGN) (5). fOSGN may be also released directly from glycoproteins and glycopeptides by the direct action of ENGase (6). fOSGN spe-cies are converted into a $Man_5GlcNAc_1$ (Manα1–2, Manα1–2, Manα1–3(Manα1–6)Manβ1–4GlcNAc) structure by an α-mannosidase called MAN2C1 (7–9). The $Man_5GlcNAc_1$ is finally transferred to the lysosomes via a specific ATP-depen-dent transporter to be degraded completely (10, 11) (Fig. 1*A*).

A minor part of free $Man_9GlcNAc_2$ is also liberated from the dolicholpyrophosphate anchor in the lumen of the ER during the biosynthesis of *N*-linked glycans and then translocated to the cytosol, where it is reduced to $Man_5GlcNAc_1$ by the con-secutive action of ENGase and MAN2C1 (12, 13).

MAN2C1 is a cytosolic α-mannosidase (EC 3.2.1.24), previ-ously called NAM (neutral α-mannosidase, according to its pH optimum of 6.5) (14). MAN2C1 belongs to the glycoside hydro-lase family 38 and is able to hydrolyze α-1,2-, α-1,3-, and α-1,6-linked mannose residues (Fig. 1*B*) (12, 15). The inhibition of MAN2C1 expression in HEK-293 cells and the inhibition of MAN2C1 activity in HepG2 cells led to the accumulation of

[1] To whom correspondence should be addressed: Dipartimento di Scienze Farmaceutiche, University of Perugia, Perugia 06126, Italy. Tel.: 39-075-5857907; Fax: 39-075-5857904; E-mail: tbeccari@unipg.it.

[2] The abbreviations used are: ER, endoplasmic reticulum; ERAD, endoplasmic reticulum-associated degradation; fOS, free oligosaccharide(s); ENGase, β-endo-*N*-acetylglucosaminidase; Man2c1, α-D-mannosidase; ES, embry-onic stem.
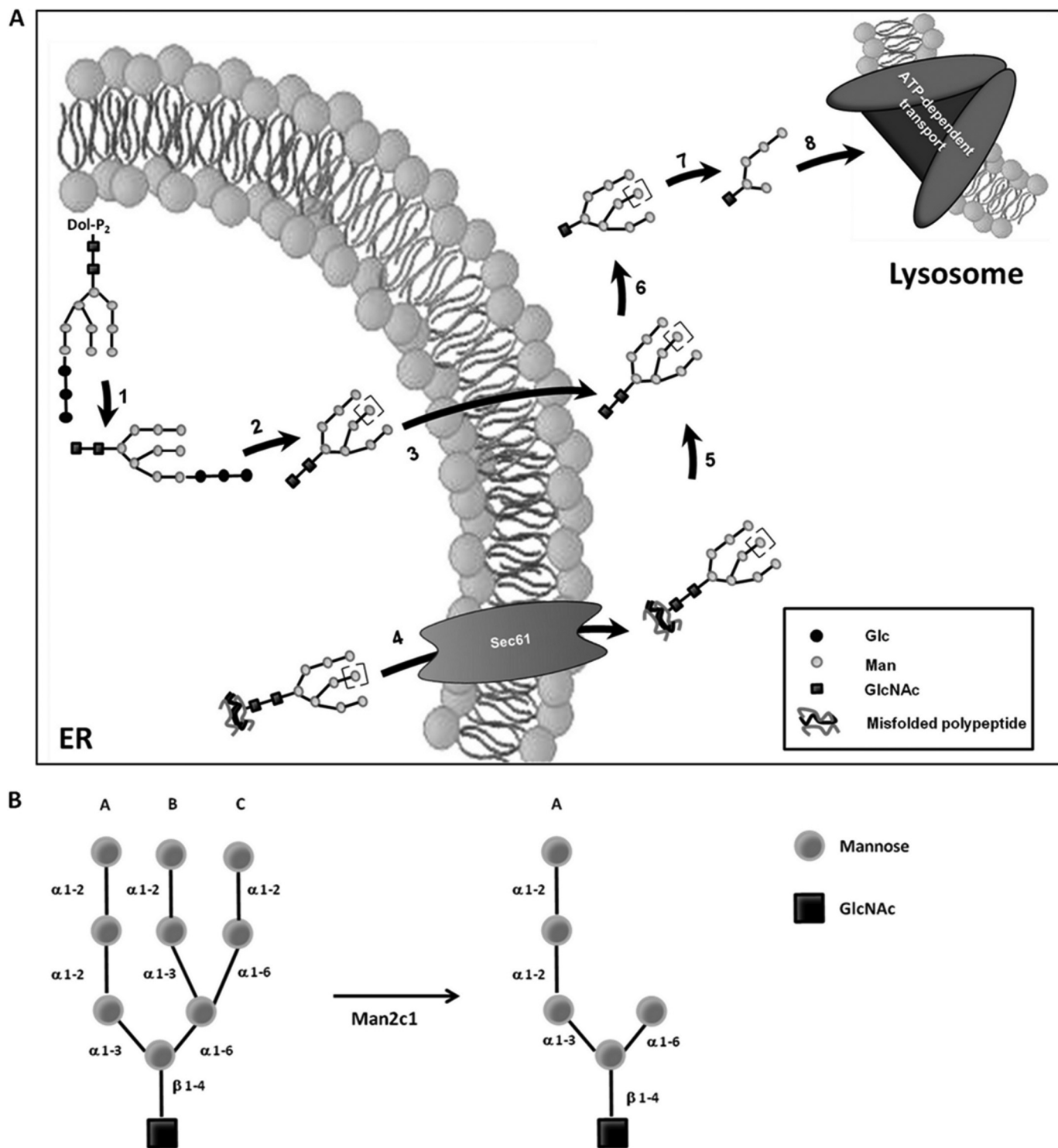
FIGURE 1. **Neutral free oligosaccharides formation and processing.** *A*, generation and trimming of fOS. fOS can be generated either in the lumen of the ER or in the cytosol during the ERAD process. $Glc_3Man_9GlcNAc_2$ is released from the dolichol pyrophosphate (Dol-PP) anchor in the lumen of the ER by the action of an oligosaccharyltransferase (*1*). α-Glucosidase I and II remove the Glc residues from fOS (*2*), which are then translocated into the cytosol (*3*). Misfolded glycoproteins originating in the lumen of the ER move to the cytosol to be degraded (*4*). An *N*-glycanase (PNGase) cleaves the *N*-linked glycans (*5*), which are reduced to $Man_9GlcNAc$ by an ENGase (*6*). $Man_9GlcNAc$ is then trimmed down to $Man_5GlcNAc$ by Man2c1 (*7*) prior to transfer into the lysosome (*8*). *B*, $Man_9GlcNAc$ cytosolic processing. The removal of mannose residues from $Man_9GlcNAc$ is carried out by Man2c1. This enzyme specifically hydrolyzes the α-1,2, α-1,3, and α-1,6 mannose residues linked to the B and C branches of fOS, giving rise to $Man_5GlcNAc$ oligosaccharides.

$Man_{8-9}GlcNAc$ oligosaccharides in the cytosol (9, 16). In line with these data, the overexpression of this enzyme caused the decrease of free high mannose-type sugars in COS cells (17). Furthermore, the overexpression of MAN2C1 in HeLa cells led to modifications of the cytosolic pool of free oligomannosides and resulted in the accumulation of small $Man_{2-4}GlcNAc_1$ oligosaccharides in the cytosol (18). This accumulation was shown to be correlated with incomplete protein glycosylation

and truncated lipid-linked glycosylation precursors, which yields an increase in *N*-glycoprotein en route to the ERAD.

Recently, MAN2C1 has been implicated in the growth of tumor cells and malignant transformation processes in cancer cells. Indeed, this protein seems to promote the tumorigenesis in human prostate cancer cells by activating the AKT pathway as a result of PTEN-negative regulation (19). Moreover, the suppression of *MAN2C1* expression resulted in mitotic arrest and apoptosis of esophageal carcinoma cells *in vitro* (20). On the other hand, *hMAN2C1* transgenic mice showed an increase in growth, invasion, and metastasis of implanted cancer cells (21).

To deepen the knowledge of the biological significance of Man2c1 and its implication in the cytosolic catabolism of fOS, we generated a *Man2c1* knockout mouse model by gene disruption. These mice did not show a visible macroscopic phenotype or behavioral alterations despite a considerable accumulation of Man$_{8-9}$GlcNAc and significant defects visible in several organs at the microscopic level.

EXPERIMENTAL PROCEDURES

Construction of a Targeting Vector and Generation of KO Mice

The murine gene encoding Man2c1 spans about 11.5 kb from the transcription initiation site to the RNA cleavage site and contains 26 exons. It is ubiquitously expressed in mouse tissues and codes a protein of 1039 amino acids (17). To disrupt the mouse *Man2c1* gene, a 5.7-kb XhoI DNA fragment containing exons 4–14 was subcloned from the Mouse Genomic λ FIX II library (Stratagene) into pBlueScript-SK$^-$ (Stratagene). The neomycin phosphotransferase gene (*neo*) was inserted in exon 7 in the SalI site to interrupt the coding sequence of the gene (Fig. 2*A*). The entire cassette was sequenced. The recombinant vector was linearized with NotI and introduced into HM-1 murine embryonic stem (ES) cells (22) by electroporation (Bio-Rad Gene Pulser II, 0.8 kV, 3 μF). After positive selection using G418-containing medium, the ES cell clones were picked, expanded, and screened by PCR. The wild-type allele resulted in the detection of a 2500-bp fragment, whereas a 3000-bp fragment occurred for the mutated allele. Primers and PCR conditions were as follows: Man2c1for, 5′-CCCTTCAAGGA-GACTGTGAGG-3′; Man2c1rev, 5′-TGGAACTGGTTGAG-GAGCAGG-3′; NEOREV, 5′-ACTTCGCCCAATAGCAGC-CAG-3′; denaturation at 98 °C for 3 min; 35 cycles of 30 s at 98 °C, 30 s at 64 °C, and 90 s at 72 °C; and 3 min at 72 °C. In targeted ES clones, the homologous recombination was reconfirmed by Southern blot analysis by using a 600-bp 3′ probe. Two recombinant ES clones were microinjected into C57BL/6N blastocysts and transferred into pseudopregnant females. The resulting chimera males, with a high contribution of agouti coat color, were backcrossed five times to C57BL/6N females. The heterozygous mice were intercrossed to generate homozygous *Man2c1*$^{-/-}$ mice. Mice were genotyped by PCR analysis of genomic tail DNA under the same conditions as described above.

To perform a quick screening of the mutated mouse progenies, different PCR conditions were used. The Man2c1rev and NEOREV primers were substituted with the following: Man2c1rev1, 5′-ACCAGGGTACTGGCTCTTGAC-3′ and NEOFOR, 5′-CAGGATGATCTGGACGAAGAG-3′, whereas the primer Man2c1for was maintained. The PCR reaction was modified as follows: denaturation at 98 °C for 3min; 40 cycles of 30 s at 98 °C, 30 s at 64 °C, and 15 s at 72 °C; and 1 min at 72 °C. Under these conditions, a 280-bp fragment for the WT and a 950-bp fragment for the KO were obtained.

Mice used in this study were housed under standard conditions in a 12-h light-dark cycle with food and water *ad libitum*. All experiments were carried out in accordance with local and state regulations for research with animals.

Enzyme Assays

Kidney, liver, brain, lung, heart, and spleen extracts were prepared from 16 week-old *Man2c1*$^{-/-}$, *Man2c1*$^{+/-}$, and WT mice. Mouse tissues were homogenized in 10 mM HEPES buffer containing 5 mM MgCl$_2$, 150 mM KAc, and 0.25 M sorbitol (pH 7.4) (1:10 w/v) and centrifuged at 16,000 × *g* for 10 min. Man2c1 and lysosomal α-mannosidase activities were determined using 3 mM fluorogenic substrate 4-methyl-umbelliferyl-α-D-mannopyranoside (Sigma-Aldrich) in 0.1 M citric acid/0.2 M disodium phosphate buffer (pH 6.5 and 4.5, respectively). Lysosomal β-mannosidase activity was also measured using 3 mM 4-methyl-umbelliferyl-β-D-mannopyranoside (Sigma-Aldrich) in the same buffer. The reactions were stopped with 0.2 M glycine/NaOH buffer (pH 10.4). The fluorescence of the liberated 4-methyl-umbelliferone was measured by using a Versa-Fluor fluorometer (Bio-Rad) (λ$_{excitation}$, 360 nm; λ$_{emission}$, 446 nm). Cathepsin D and cathepsin E activities were determined by incubating samples with 30 μM MOCAc-Gly-Lys-Pro-Ile-Leu-Phe-Phe-Arg-Leu-Lys(Dnp)-D-Arg-NH$_2$ (Enzo Life Sciences) dissolved in 50 mM sodium acetate buffer (pH 4.0) at 40 °C in the presence and absence of the cathepsin D inhibitor pepstatin A (15 μM). Reactions were stopped by adding 5% (w/v) trichloroacetic acid and measured fluorimetrically (λ$_{excitation}$, 328 nm; λ$_{emission}$, 393 nm). The amount of protein was quantified using Bradford reagent (Bio-Rad) (23).

Western Blot Analysis

40 μg of proteins from *Man2c1*$^{+/+}$, *Man2c1*$^{+/-}$, and *Man2c1*$^{-/-}$ mouse tissue extracts were suspended in reducing sample buffer, boiled for 5 min, and loaded on a 7% SDS-PAGE gel. Proteins were electrophoretically transferred to a nitrocellulose membrane and blocked with 5% nonfat milk in Tris-buffered saline and Tween 20 solution (TBS-T). Man2c1 was detected by using a goat anti-Man2c1 antibody (catalog no. sc-66458, Santa Cruz Biotechnology) followed by a secondary antibody. The immunoblot was visualized by chemiluminescence (Immobilon Western, Millipore) on Hyperfilm x-ray film.

Histology

Paraffin Histology and Immunohistochemistry/Lectin Histochemistry—16-week-old mice were killed by an overdose of anesthetic and then perfused sequentially via the left ventricle with 20 ml of phosphate buffer with 1% procaine HCl and then either modified Bouin's solution (24) or neutral buffered formaline (Sigma-Aldrich). After dissection and embedding of indi-

vidual organs in paraplast, sections were cut at a thickness of 7–10 μm and mounted on aminosilane-coated slides. After deparaffinization in xylene and rehydration in a graded series of ethanols, sections were either used for a routine H&E stain according to standard protocols or blocked with a mixture of 5% BSA and 5% non-immune serum and then incubated overnight with the primary antibody according to the instructions of the manufacturer. Alternatively, to avoid extraction of cell constituents (especially lipid compounds), fixed organs were encased in agarose and cut on an Leica VT 1200 S high-frequency vibratome prior to staining. After the detection of primary antibody binding via fluorochrome-conjugated secondary antibodies (Alexa Fluor 488 or Alexa Fluor 549), samples were documented with a motorized Nikon 90i microscope equipped with a triple-color eZC1 confocal laser unit.

For lectin histochemistry, sections from samples fixed in modified Bouin's solution were reacted with concanavalin A, *Lens culinaris*, and *Pisum sativum* lectins to detect enrichment of mannose residues in different tissues. To increase lectin staining sensitivity, parallel samples were fixed by immersion rather than perfusion fixation, reducing the loss of fOS from histological material. Additional lectin stains were performed with *Ricinus communis* agglutinin 1 to identify activated microglia as well as with *Griffonia simplicifolia* agglutinin II, known to detect glycogen with a significantly higher sensitivity than classical periodic acid-Schiff stains (25). Positive lectin staining signals were confirmed by transmission electron microscope as an independent method control (see below).

High-resolution Light Microscopy—Mice were killed as described above and perfused transcardially with first 20 ml of Sörensen phosphate buffer with 1% procaine HCl, followed by 6% glutardialdehyde dissolved in the same buffer, again with 1% procaine HCl. Samples were dissected from individual organs, postfixed in 2% OsO_4 for lipid retention, and embedded in Spurr resin in the ERL 4221D variant, according to standard protocols, using propylene oxide as an intermediate. Sections of 1 μm were cut on a Powertome® ultramicrotome, mounted on glass slides, and stained with either toluidine blue/pyronin G or p-phenylene diamine, the latter being employed as a sensitive lipid stain.

Transmission Electron Microscopy—Regions of interest of about 1 mm^2 were identified on the semithin sections and prepared as described above. The respective Spurr resin blocks were then trimmed down with a diamond milling cutter and resectioned at 70 nm. Sections were collected on 300 mesh copper grids, contrasted with lead citrate and uranyl acetate, and documented in a Zeiss EM 910 transmission electron microscope equipped with a Tröndle 4 MP digital camera.

Extraction and Analysis of Soluble Oligosaccharides

Extraction of Soluble Oligosaccharides—Tissues of WT and *Man2c1* KO mice were dilacerated in an ice-cold KMH buffer (110 mM potassium acetate, 2 mM magnesium acetate, and 20 mM HEPES (pH 7.2)) containing a protease inhibitor mixture (cOmplete, Roche Diagnostics). Cellular homogenization was performed by using a Potter-Elvehjem homogenizer (750 rpm, 5 strokes). The cellular homogenate was then submitted to lipid extraction by addition of methanol and chloroform (MeOH/ $CHCl_3$/tissue extract in a ratio of 3/2/1, v/v/v) (26). The aqueous phase containing free oligosaccharides and resulting from the lipid extraction was then lyophilized.

Permethylation of Oligosaccharides—Permethylation of the freeze-dried oligosaccharides and sample cleanup were performed as described previously (27). Internal standard maltoheptaose was permethylated with triply deuterated iodomethan under the same conditions.

MALDI TOF-MS Analysis—For each sample, permethylated oligosaccharides were mixed with a known amount of maltoheptaose standard. MALDI-MS experiments were carried out on a Voyager Elite DE-STR Pro instrument (PerSeptive Biosystem, Framingham, MA) equipped with a pulsed nitrogen laser (337 nm) and a gridless delayed extraction ion source. The spectrometer was operated in positive reflectron mode by delayed extraction with an accelerating voltage of 20 kV, a pulse delay time of 250 ns, and a grid voltage of 72%. All spectra represent accumulated spectra obtained by 500 laser shots. For each sample, three samples were spotted, and the amount of each oligosaccharide was quantified by calculating the ratio between the relative amount of these oligosaccharides and the internal standard in the MALDI-MS spectra. Protein concentration of tissue samples was measured by a micro BCA protein assay reagent kit (Pierce).

RESULTS

Generation of Man2c1-deficient Mice

To generate a *Man2c1* KO mouse model, a gene targeting vector was created (Fig. 2*A*) and used to disrupt the cytosolic α-mannosidase gene by homologous recombination in ES cells. Following drug selection, 6 of 100 ES cell clones screened by PCR analysis indicated homologous recombination. Southern blot analysis of EcoRI-digested genomic DNA resulted in a 12-kb EcoRI fragment of the WT allele and a 5-kb specific fragment of the recombinant allele, confirming the disruption of the *Man2c*1 gene in all of these clones (Fig. 2*B*).

Two recombinant ES clones were injected into C57BL/6 blastocysts. Male chimeras were identified by agouti coat color and backcrossed with wild-type C57BL/6 females. Heterozygous mice were identified by PCR and intercrossed to generate homozygous mice, which represented the 25% of the F2 offspring, as expected. Genotyping of these mice was carried out by PCR analysis (Fig. 2*C*).

Man2c1$^{-/-}$ mice were fertile. They appeared normal and did not show any difference in growth, weight, or lifespan up to 12 months when compared with wild-type mice.

Enzyme Activity

α-Mannosidase activity was measured in the kidney, liver, brain, lung, heart, and spleen of 16-week-old KO, heterozygous, and WT mice at both neutral and acid pH. Almost no neutral activity was found in KO tissues (in Fig. 3*A*, results obtained with liver and kidney are shown; similar results were achieved with the other tissues), whereas in heterozygous mice, ~50% of the wild-type enzyme activity was detected. The activity at pH 4.5 was similar in all mice and most likely reflects the activity of lysosomal mannosidases with an acidic pH optimum.

To evaluate whether the endosomal-lysosomal system was enhanced as a consequence of oligosaccharides accumulation, β-mannosidase, cathepsin D, and cathepsin E activities were also
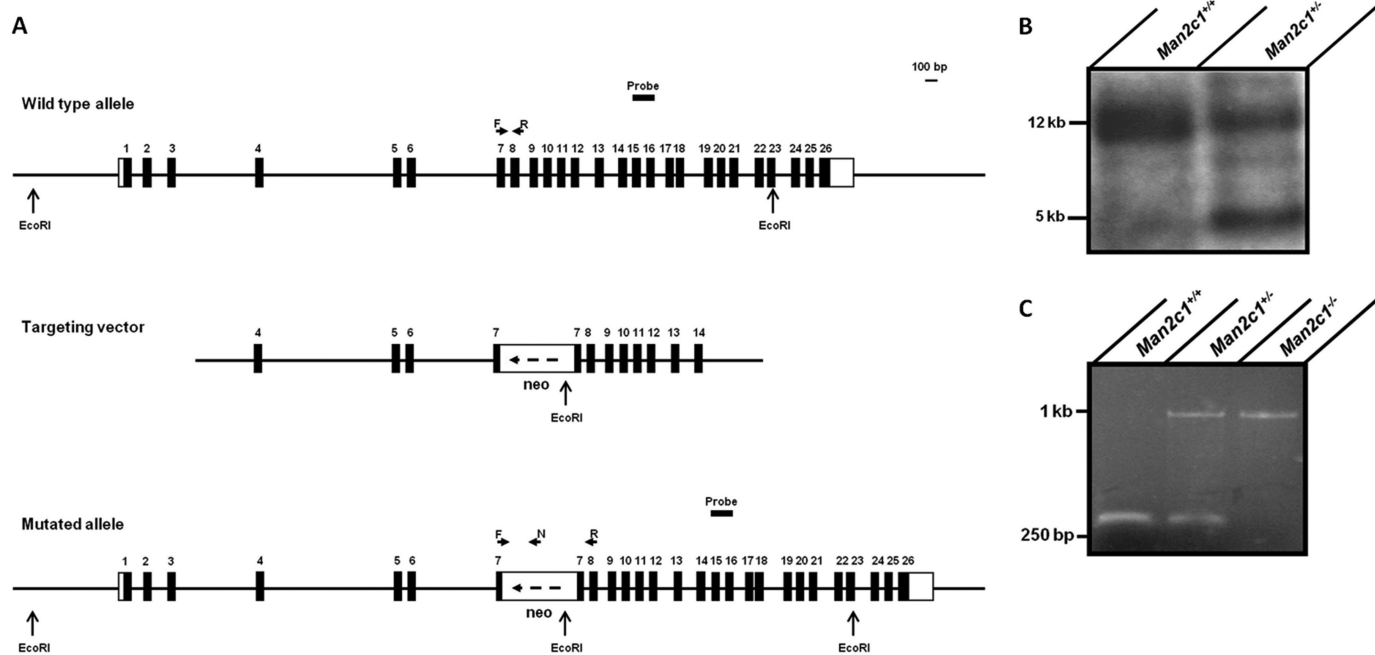
FIGURE 2. **Strategy for disruption of the *Man2c1* gene.** *A*, schematic of targeted inactivation of the *Man2c1* gene by homologous recombination in ES cells. *Boxes* depict exons. *Black parts of boxes* correspond to coding regions and *white parts* to non-coding-regions of the *Man2c1* gene, respectively. The pBlueScript-SK⁻ targeting vector has a neomycin resistance cassette inserted into exon 7 (the *arrow* within the neo cassette indicates transcriptional orientation). The 3′ probe used for Southern blot analysis of recombinant ES clones as well as the primers used to screen mouse litters are indicated. *F*, Man2c1for; *R*, Man2c1rev1; *N*, NEOFOR. *B*, Southern blot analysis of wild-type and recombinant ES clones. Genomic DNA was digested with EcoRI, separated on an agarose gel, blotted, and hybridized with the 3′ probe. The 12-kb fragment corresponds to the WT allele, and the 5-kb fragment corresponds to the mutated allele. *C*, PCR genotyping of mouse tail DNA. Rapid genotyping was performed using the primers F, R, and N. The 280-bp fragment corresponds to the WT allele, whereas the 950-bp fragment corresponds to the KO allele.
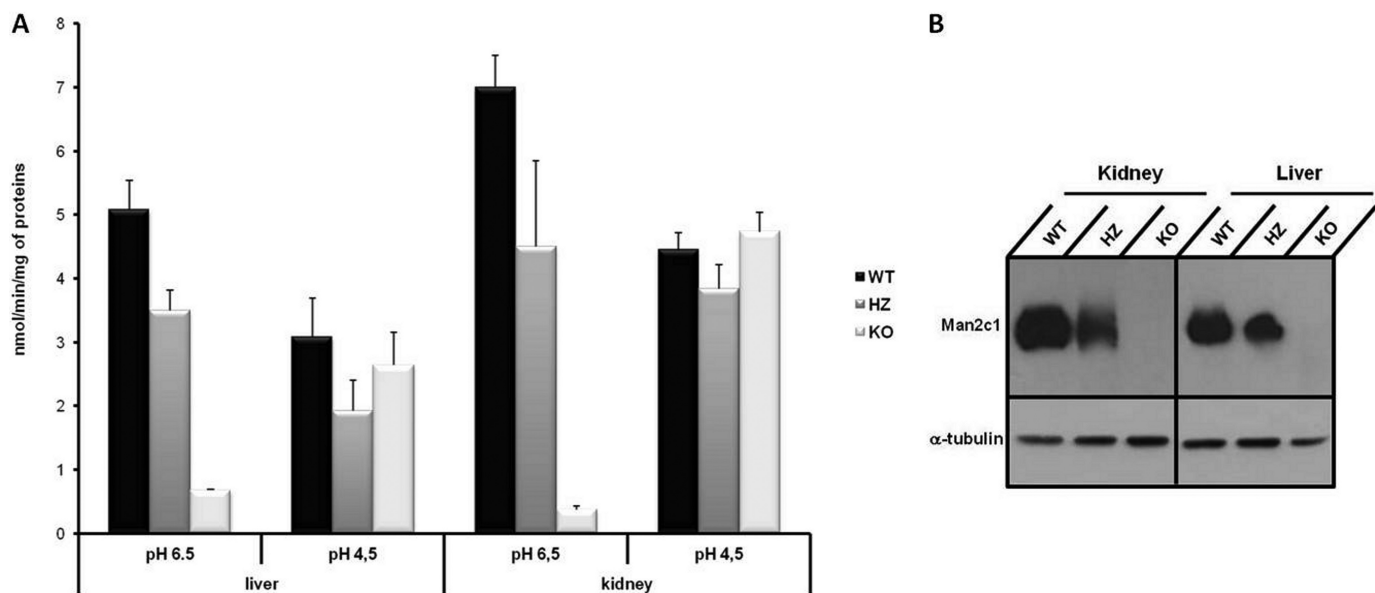

FIGURE 3. **Evidence of Man2c1 deficiency.** *A*, neutral (pH 6.5) and acid (pH 4.5) α-mannosidase activity assayed in WT, heterozygous (*HZ*), and KO mouse liver and kidney. For each group, three 16-week-old mice were analyzed. *Error bars* represent 1 S.D. Enzyme activity was expressed as nanomoles/minute/milligram of protein. *B*, Western blot analysis of Man2c1 in WT, heterozygous, and KO liver and kidney extracts. α-Tubulin was used as an internal control.

measured in the kidney, liver, brain, lung, heart, and spleen. Comparable values between KO and WT animals were observed in all analyzed tissues (data not shown).

Western Blot Analysis

The deficiency of Man2c1 in KO mice was confirmed by immunoblotting analysis. The amount of protein in heterozygous tissues was reduced with respect to WT counterparts (in Fig. 3*B*, the result obtained with liver and kidney is shown).

Oligosaccharide Analysis

To obtain functional evidence of *Man2c1* knockout, we quantified and compared the structure of free oligomannosides in various tissues of WT and KO male and female mice. Free oligosaccharides were extracted from tissue homogenates and permethylated prior to analysis by MALDI-TOF MS. WT tissues presented a very low-level population of free $Man_{2-5}GlcNAc_1$ (Fig. 4, *A* and *B*). These populations represent
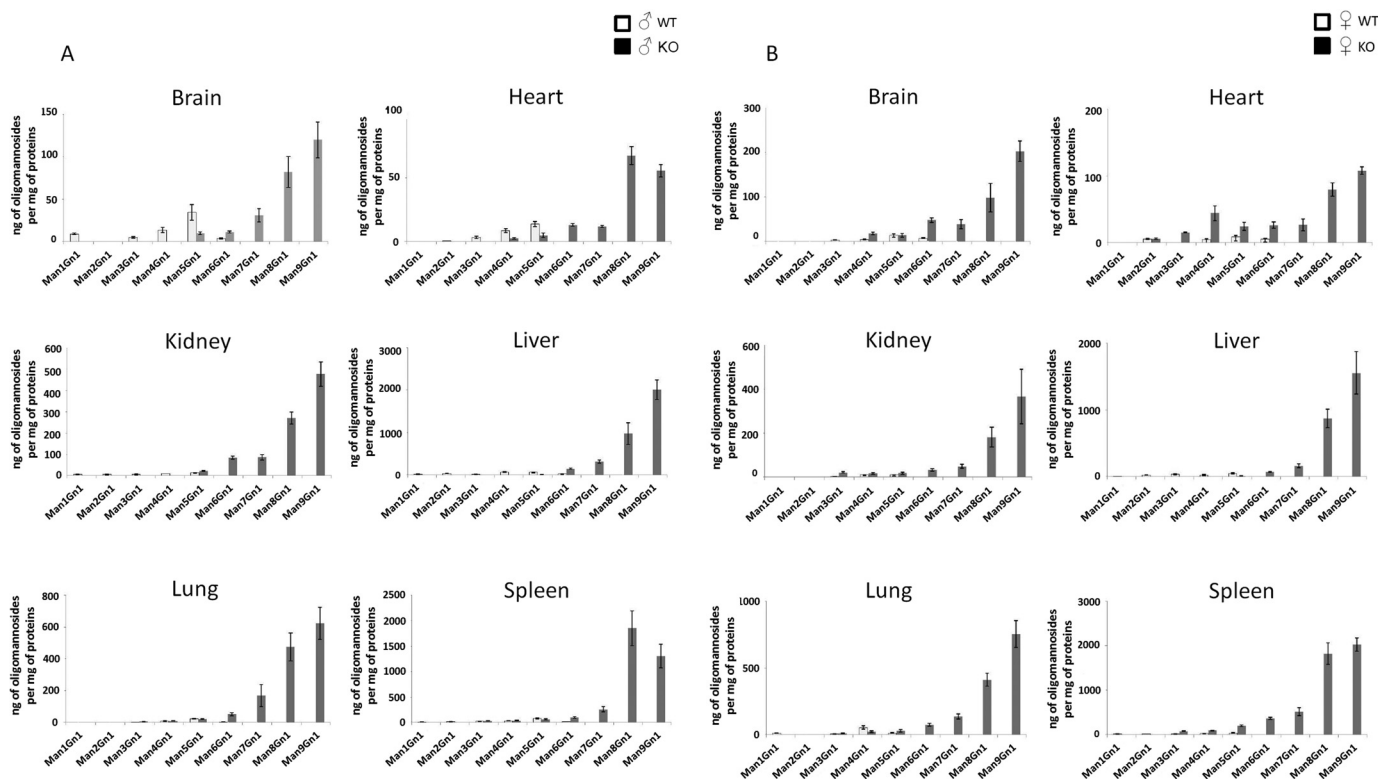
FIGURE 4. **Quantitative analysis of free oligomannosides released in WT and *Man2c1* KO mouse tissues.** *A*, KO versus WT male tissues. *B*, KO versus WT female tissues. Free oligosaccharides were extracted from male and female WT and *Man2c1* KO mice tissues as described under "Experimental Procedures." Oligosaccharides were permethylated and mixed with 5 ng of permethylated standard. Quantification of oligosaccharides was performed by calculating the ratio of peak height, taking the standard as a reference. The values were normalized to the quantity of proteins in milligrams. For all assays, values are the mean ± S.D. of three independent experiments.

the steady-state level of free oligomannosides originating from the ERAD process. In contrast, a clear accumulation of higher oligomannosides species, particularly $Man_{8-9}GlcNAc_1$, was observed in *Man2c1* KO mouse tissues (Fig. 4, *A* and *B*). Their abundance is consistent with the function of the Man2c1 because they represent the specific substrates of the KO enzyme. However, the presence of smaller species ($Man_1GlcNAc_1$ to $Man_7GlcNAc_1$) indicates that another cellular α-mannosidase was able to trim Man2c1 substrates. Interestingly, we observed that the accumulation of $Man_{8-9}GlcNAc_1$ species was tissue-specific. They were more abundant in the liver and spleen and less represented in the brain and heart. Because KO mouse models of lysosomal glycosidases were often accompanied by the presence of oligosaccharides in urines, we checked their presence in *Man2c1* KO mice urine, but no trace of oligomannosides was detected (data not shown).

Histological Findings

A screen of α-mannosidase knockout tissues revealed major histopathological changes in several organs (Fig. 5) where the liver, small intestine, kidney, and CNS featured the most impressive alterations. Somewhat in contrast to the tissue distribution of oligosaccharide accumulation, we did not observe major defects in spleen tissue.

CNS—Within the isocortex (Fig. 5, *A* and *B*), we observed neuronal degeneration mainly in layer V, *i.e.* among subcortically projecting neurons. Within layer V, a significant proportion of large, *i.e.* pyramidal, neurons feature multiple vacuoles

that mostly appear clear and empty but, in some cases, may be filled with intensely basophilic staining material. Interestingly, these vacuoles predominantly concentrate around the basal (axonal) aspect of the cell so that the dendritic tree, even in otherwise severely affected cells, may appear unchanged.

Next to the isocortical lamina V, the major CNS white matter tracts (corpus callosum, fimbria hippocampi, internal capsule, and hemispheral subcortical white matter) (Fig. 5, *C* and *D*) feature lesions in the form of multiple irregular patches of about 100- to 200-mm diameter, characterized by vacuolated (oligodendro) glial cells. Although here the vacuoles extend into the proximal parts of the glial processes, the myelin sheaths still appear normal, at least in high-resolution light microscopy on semithin sections of epoxy resin-embedded material. Within these patches, activated microglial cells can be revealed by RCA1 staining, and affected cells feature an increased stainability with mannose-binding lectins. Interestingly, such white matter defects were not observed in other regions of the CNS, like the cerebellum (data not shown).

Liver—In the livers of α-mannosidase-deficient mice (Fig. 5, *E–H*), numerous hepatocytes appear swollen, featuring an abnormally pale cytoplasm studded with mitochondria (Fig. 5, *G* and *H*). The presence of large amounts of glycogen and cellular edema could be confirmed by electron microscopy (Fig. 5, *I–L*). Interestingly, the mitochondria themselves were not affected, and dilated profiles of rough endoplasmic reticulum (RER) were only encountered occasionally, mainly in cells still
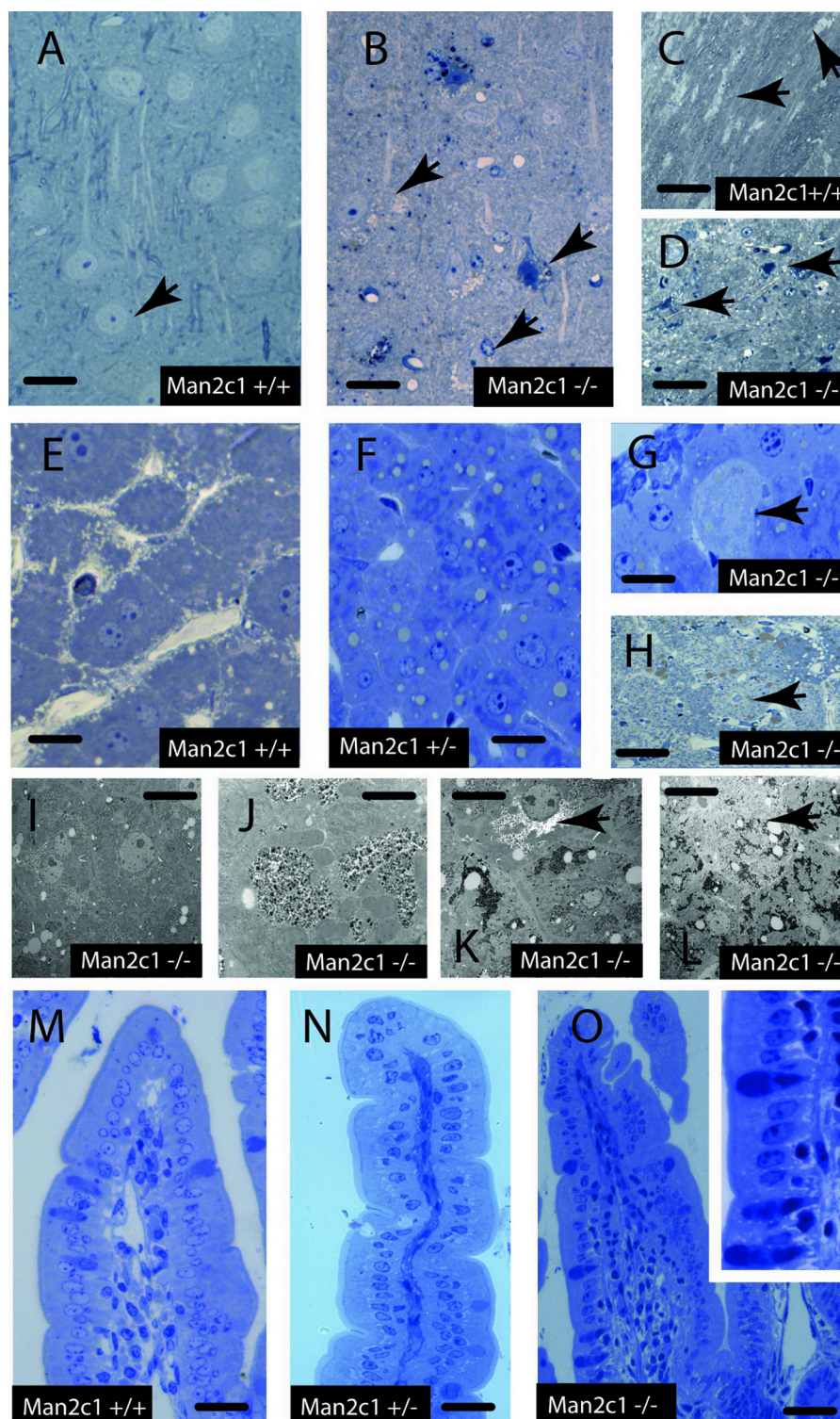
FIGURE 5. **Key lesions of Man2c1-deficient mice shown in semithin resin sections stained with toluidine blue and pyronine G.** In contrast to wild-type isocortex lamina V (*A*), pyramidal neurons in KO lamina V (*B*) feature major vacuolation around their basolateral aspect (compare *arrows* in *A* and *B*), typically sparing the dendritic compartment, thus arguing for a specific vulnerability of adaxonal protein synthesis for Man2c1 deficiency. *C* and *D*, the subcortical white matter of WT (*C*) and KO (*D*) mice. Note again the vacuolation in oligodendroglia in KO mice (*C* and *D*, *arrows*). *E–H*, morphology of hepatocytes in WT (*E*), heterozygous (*F*), and KO (*G*) mice is compared in semithin sections. Note the accumulation of lipid droplets in heterozygous mice (*F*) and the occurrence of unusually pale cells in knockout livers (*G* and *H*, *arrows*). Note that, in these pale cells, the cytoplasm is segregated by staining characteristics, featuring spots of dark basophilic material (*H*, *arrow*). Transmission electron microscopy on KO livers (*I–L*) showed a high glycogen content in these cells (*I* and *J*), accompanied by cellular edema (*K* and *L*), explaining the occurrence of pale cells in light microscopy. Likewise, we compared the morphology of the small intestine in all three genotypes (*M–O*). Note that, at low magnification detailing the entire intestinal villi, especially WT and heterozygous tissue did not reveal visible differences. Only KO villi of the small intestine featured an irregular basal border of enterocytes, characterized by multiple retronuclear vacuoles and invading lymphocytes (*O* and *inset*). *Scale bars* = 20 μm (*A—D*); 15 μm (*E*, F, and *H*); 10 μm (*G*); 5 μm (*I—L*); 15 μm (*M—O*).

appearing normal by other criteria. Both in affected and still normal-appearing cells, droplets filled with material that exhibited staining characteristics compatible with lipids and bile constituents were detected. They were located next to some clear vacuoles and could be indicative of microcholestasis next to a significantly more prevalent lipid accumulation. A more frequent occurrence of lipid droplets was already seen in heterozygous mice. Lectin histochemistry revealed groups of hepatocytes predominantly situated at the periphery of lobuli, featuring increased stainability with both mannose- and glycogen-binding lectins. Similar to the situation in enterocytes, increased lectin staining without overt cell degeneration was, to a smaller degree, also observed in heterozygous mice (not shown).

Small Intestine—Within the small intestine and especially within the duodenum (Fig. 5, M–O), numerous large clear vacuoles piling up in a mainly retronuclear (*i.e.* basal) position in the cells were seen already at the light microscope level, an effect not seen in heterozygous mice. Moreover, lymphocytes were seen to invade the basal region of the gut epithelial layer (Fig. 5O, inset). In contrast, the apical cell region, including the brush border, was not visibly affected by vacuole formation and, besides the glycogen stores (see below), even features a normal ultrastructure.

Enterocytes in knockout animals are characterized by an increased stainability of the supranuclear cytoplasm and, partly, the brush border by mannose-binding lectins as well as lectins detecting glycogen. Interestingly, this effect also occurred in enterocytes of heterozygous mice (Fig. 6, A–F). The presence of significant amounts of glycogen could be verified by transmission electron microscopy (Fig. 6, G and H). Within the villus stroma, these changes are accompanied by dilated intracellular spaces and an increased density of macrophages situated between blood vessels and lymphatics.

Kidney—We observed a small number of scattered individual glomeruli being collapsed, *i.e.* having reduced or lost lumina of both capillaries and Bowman's space. Some of the still normal-appearing glomeruli featured a moderate fibrosis visible mainly by transmission electron microscopy, with collagen bundles and fibroblasts lined up around the outer leaflet of Bowman's capsule (Fig. 6, O–Q). Increased lectin stainability, albeit at variable intensity, was mainly observed in the epithelia of proximal tubules, which, however, displayed a normal ultrastructure.

Oligosaccharide Accumulation—In general, the lectin data corroborate the accumulation of mannosyl compounds in different tissues and also reveal conspicuously high levels of glycogen in cell types capable of gluconeogenesis. In addition, we sometimes noticed increased lectin binding in the microvascular endothelia of different Man2c1-deficient tissues (Fig. 6, I–N), most notably in the heart and liver. That could be indicative of an increased transendothelial transfer of accumulated saccharides. Interestingly, a limited accumulation was also observed in heterozygous tissues, albeit without the signs of cellular degeneration seen in the respective KO cells.

DISCUSSION

Free $Man_{7-9}GlcNAc_2$ can be released from dolicholpyrophosphate-linked oligosaccharides during the biosynthesis pathway of N-linked glycans or from misfolded glycoproteins throughout the ERAD process. In the cytosol, fOS are reduced to $Man_5GlcNAc$ to enter into the lysosomes and be degraded completely (12).

Until now, the *in vivo* consequences because of the loss of activity of the enzymes involved in the cytosolic trimming of fOS were unknown. Here we describe the effects caused by the lack of the cytosolic α-mannosidase by the generation of a *Man2c1* KO mouse line.

Man2c1-deficient mice were fertile and showed a normal appearance up to the age of 1 year. Notably, no skeletal or gross neurological abnormalities characteristic for deficiency of lysosomal mannosidases were observed. However, a detailed analysis revealed the presence of less obvious biochemical and histological alterations in several tissues.

The accumulation of $Man_{8-9}GlcNAc$ oligosaccharides was recognized in the brain, heart, kidney, liver, lung, and spleen of KO mice. A quantitative analysis showed higher levels of fOS in the spleen and liver when compared with the other analyzed KO tissues (Fig. 4, A and B). Their presence can reflect the transport of $Man_{8-9}GlcNAc$ from the cytosol into the lysosomes via the ATP-dependent transporter (10, 11). Even if oligosaccharide import was selective toward partially demannosylated fOS, the presence of one GlcNAc residue at the reducing end was described to be of critical importance for its interaction with the ATP-dependent transporter. When transported into the lysosomes, the degrading process of $Man_{8-9}GlcNAc$ can be carried out by the acidic α- and β-mannosidases. However, accumulated $Man_{1-7}GlcNAc$ could derive from the alternative route followed by some misfolded glycoproteins. These molecules pass from the ER to the Golgi complex, where α1,2mannosidases and/or endo-α-mannosidases act on the N-linked oligosaccharides (16). The resulting glycoproteins are then recycled back to ER and submitted to ERAD targeting, producing fOS (12, 28). Alternatively, $Man_8GlcNAc_1$ and $Man_9GlcNAc_1$ compounds could be transported by a nonspecific mechanism from the cytosol into the lysosomes, where the degrading process can be carried on by the acidic α-mannosidase. However, the activity of some lysosomal enzymes (α-mannosidase, β-mannosidase, and cathepsin D) and the endosomal enzyme cathepsin E in 16-week-old *Man2c1*-deficient mice was similar to that in WT littermates. This does not support the hypothesis of an endosomal-lysosomal system activation.

Lectin and transmission electron microscope analysis of glycan storage, on one hand, confirmed data from biochemical analysis but also revealed two further aspects, *i.e.* the small-scale accumulation in heterozygous tissues and the presence of conspicuously large amounts of glycogen next to mannosyl compounds, whereby the latter effect seems to be restricted to cells capable of gluconeogenesis (for enterocytes, see Ref. 29). The small-scale accumulation of mannosyl compounds in heterozygous tissues may be seen in accord with the significantly reduced amount of enzyme protein described here, driving cells to the verge of haploinsufficiency. Likewise, we observed degenerative effects on cells only in the knockout material, in line with a loss-of-function effect.
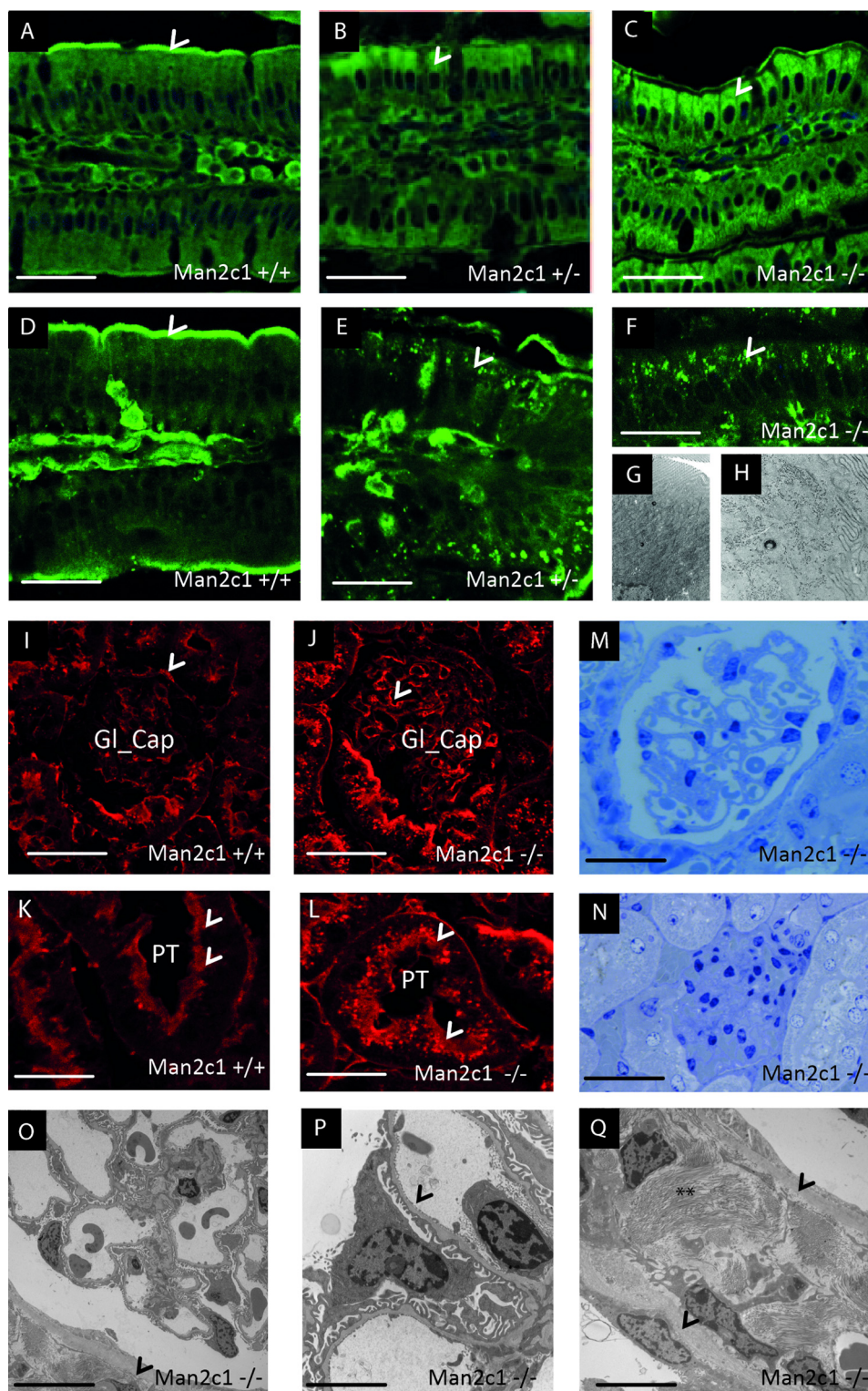
FIGURE 6. **Increased lectin binding reveals accumulation of mannose- or GlcNAc-containing saccharides in KO tissues.** Comparing WT (*A*), heterozygous (*B*), and KO (*C*) enterocytes, we show that enrichment of these compounds is already visible in the supranuclear portion of heterozygous enterocytes, similar to knockout cells (*C*). This accumulation is paralleled by an enrichment of glycogen, as shown by both lectin histochemistry (*D–F*) and electron microscopy (*F*, *G*, and *H*). In the kidney (*I–N*), lectins recognizing mannosyl compounds featured next to intensely staining glomerular capillaries (*Gl_Cap*). Multiple, intensely staining dots probably corresponding to lysosomes are visible in KO proximal tubules (*PT*). Although most of the glomeruli in KO kidneys featured a normal appearance in light microscopy (*M*), individual units looked collapsed (*N*), with erythrocytes blocked within capillaries. Transmission electron microscopy featured a normal overall morphology of uncollapsed glomerula with a normal morphology of endothelia and podocytes (*P*, *arrowhead*) but featuring a conspicuously thick basal lamina around the outer leaflet of Bowman's capsule (*O* and *Q*, *arrowheads*), thick bundles of collagen (*Q*, *double asterisk*), and the deposition of a multilayered basal lamina-like material around adjacent blood vessels (*O* and *Q*, *arrowheads*). Scale bars = 20 μm (*A—E*), 15 μm (*F*), 50 μm (*I, J, M*, and *N*); 20 μm (*K* and *L*), 20 μm (*O*), 5 μm (*P* and *Q*).

Cytosolic α-D-Mannosidase (Man2c1)-deficient Mice

The relatively high glycogen content of knockout cells, in turn, may be explained by the bidirectional regulation of gluconeogenesis by ER stress responses (30–32), whereby glycogen formation could simply be a method to reduce intracellular osmotic pressure created by a surplus of glucose. Because accumulation of mannose-containing fOS in the cytoplasm, occurring both in *Man2c1* knockout as well as overexpressing cells (this work and Ref. 18) has been linked to the activation of an ER stress response, glucose/glycogen accumulation may be a rather straightforward response to mannosyl fOS enrichment or defects of their turnover.

Cellular lesions and/or outright degenerations were only seen in a few instances. Increased retronuclear vacuolization of enterocytes (*i.e.* affecting the region of the Golgi field of these cells and the nutrient extrusion site toward the blood vessels and lymphatics of the villus stroma) remain unexplained so far, the more so as they do not coincide with glycan storage, which was concentrated in the apical cell pole.

Because ER stress signals (like SEL1L, Ref. 33) have been linked to intestinal epithelial cancer progression and because Man2c1, likewise, has been reported to play a role in the progression toward an increased malignancy of prostate cancer, Man2c1-deficient mice may be a valuable model to further investigate the link between fOS-associated ER stress and epithelial tumorigenesis, *e.g.* in older mice.

A histological analysis further revealed severe changes in the CNS, kidney, and liver. In the CNS, the predominant occurrence of neuronal lesions in layer V coincides with the presence of predominantly long-axoned projection (Golgi type 1) neurons, *i.e.* cells characterized by high protein production from the rough endoplasmic reticulum to sustain their axonal projections. In contrast, other Golgi type 1 neurons in the cortex, like the small pyramidal cells of layer II/III, have comparatively short axons with associational or commissural trajectories. Therefore, it is of special interest that the vacuolization of neurons is mainly seen in their basal aspect, *i.e.* close to the axon hillock, which would coincide with an especially important role of Man2c1 with the turnover of sugar moieties from proteins destined for axonal localization, a notion supported by the localization of specific mRNAs at this site (34).

The occurrence of lesions in the subcortical white matter is also intriguing because oligodendroglia appear to be especially prone to ER stress reactions, both during development from its precursors (35) as well as in a variety of neurodegenerative disorders like Parkinson disease or multiple-system atrophy (36), *i.e.* even in conditions of primarily neuronal origin.

Degeneration of scattered hepatocytes by morphology was always associated with cell swelling, where mitochondria remained conspicuously intact, which, speculatively, may be interpreted as an osmotic origin of water influx, *e.g.* because of increased cytosolic sugar content. This interpretation would be in line with the high glycogen amounts because hepatocyte swelling (next to ER stress) is a documented strong activator of converting glucose into the osmotically less critical glycogen polymer form (37, 38). Therefore, the high protein turnover characteristic of liver parenchyma may be the ultimate reason for mannosyl compound accumulation by ERAD defects.

Comparison of the phenotype of Man2c1-deficient mice to that of mice lacking lysosomal mannosidases next to numerous differences reveals few surprising similarities. To start with the latter, vacuolation of, specifically, the basal (adaxonal) side of isocortical neurons (mainly long-axon Golgi type I cells) seen in Man2c1 deficiency (Fig. 5*B*) have been observed in a similar fashion in β-mannosidase knockouts (Fig. 4*A* in Ref. 39).

A related parallel between Man2c1 deficiency and β-mannosidosis may exist in the case of oligodendrocytes, which are vacuolated in both instances, even if these cells appear to be significantly more affected in β-mannosidosis compared with Man2c1 deficiency (39). Available biochemical data indicate that deficiency for β-mannosidase causes accumulation of disaccharides. That is, their immediate biochemical lesion is clearly distinct from that seen in Man2c1 deficiency. Thus, one might speculate that, in both conditions, the related vacuolation pattern might rather be linked to similarly sorted (*e.g.* axonal or myelin) glycoproteins, be it from ineffective synthesis and ERAD or ineffective lysosomal degradation (in the case of axons, following retrograde transport). However, despite these similarities, murine Man2c1 deficiency does not reflect the severe phenotype of bovine β-mannosidase. Strikingly, phenotypes differ significantly from lysosomal α-mannosidase deficiency, and even when similar organs are affected, like the kidney or CNS, the distribution pattern of affected cells is clearly different (40). As yet, the few but intriguing similarities between Man2c1 deficiency and β rather than α mannosidosis remain unexplained but may indicate that the identity of misdigested glycoproteins may be more important than the internal structure of the glycan moieties.

The results described in this work demonstrate the essential role of Man2c1 in the fOS degradation process. The tissue damage observed in Man2c1-deficient mice suggests that the genetic lack of this protein could cause a not-yet-described disease in humans with involvement of the CNS.

Furthermore, several reports have confirmed the association between MAN2C1 and malignant transformation processes that occur in cancer cells (19–21). MAN2C1 overexpression promoted tumor growth and metastasis of xenograft tumors in immunocompromised mice. Moreover, up-regulation of *MAN2C1* was observed in human prostate cancer cells, where MAN2C1 seemed to attenuate PTEN functions by binding to PTEN (19). Conversely, down-regulation of *MAN2C1* induced growth delay or arrest in nasopharyngeal carcinoma cells (41) and led to mitotic arrest and apoptosis in esophageal cancer cells (20). Recently, the antiapoptotic function of MAN2C1 was investigated. MAN2C1 seems to have an enzyme-independent role in the apoptotic signal mechanism. In particular, down-regulation of *MAN2C1* caused apoptosis in HeLa cells via a mitochondrion-dependent intrinsic pathway without the occurrence of ER stress (42). In this context, our model could represent a useful tool to better understand the role of Man2c1 in the apoptotic signal pathway and in tumorigenesis of various cancer types *in vivo*.

REFERENCES

1. Gauss, R., Kanehara, K., Carvalho, P., Ng, D. T., and Aebi, M. (2011) A complex of Pdi1p and the mannosidase Htm1p initiates clearance of unfolded glycoproteins from the endoplasmic reticulum. *Mol. Cell* **42,** 782–793

2. Quan, E. M., Kamiya, Y., Kamiya, D., Denic, V., Weibezahn, J., Kato, K., and Weissman, J. S. (2008) Defining the glycan destruction signal for endoplasmic reticulum-associated degradation. *Mol. Cell* **32,** 870–877

3. Suzuki, T., Park, H., and Lennarz, W. J. (2002) Cytoplasmic peptide:*N*-glycanase (PNGase) in eukaryotic cells. Occurrence, primary structure, and potential functions. *FASEB J.* **16,** 635–641

4. Hershko, A., Ciechanover, A., and Varshavsky, A. (2000) Basic Medical Research Award. The ubiquitin system. *Nat. Med.* **6,** 1073–1081

5. Cacan, R., Dengremont, C., Labiau, O., Kmiécik, D., Mir, A. M., and Verbert, A. (1996) Occurrence of a cytosolic neutral chitobiase activity involved in oligomannoside degradation. A study with Madin-Darby bovine kidney (MDBK) cells. *Biochem. J.* **313,** 597–602

6. Chantret, I., Fasseu, M., Zaoui, K., Le Bizec, C., Yayé, H. S., Dupré, T., and Moore, S. E. (2010) Identification of roles for peptide: *N*-glycanase and endo-β-*N*-acetylglucosaminidase (Engase1p) during protein *N*-glycosylation in human HepG2 cells. *PLoS ONE* **5,** e11734

7. Duvet, S., Labiau, O., Mir, A. M., Kmiécik, D., Krag, S. S., Verbert, A., and Cacan, R. (1998) Cytosolic deglycosylation process of newly synthesized glycoproteins generates oligomannosides possessing one GlcNAc residue at the reducing end. *Biochem. J.* **335,** 389–396

8. Oku, H., Hase, S., and Ikenaka, T. (1991) Purification and characterization of neutral α-mannosidase that is activated by CO^{2+} from Japanese quail oviduct. *J. Biochem.* **110,** 29–34

9. Suzuki, T., Hara, I., Nakano, M., Shigeta, M., Nakagawa, T., Kondo, A., Funakoshi, Y., and Taniguchi, N. (2006) Man2C1, an α-mannosidase, is involved in the trimming of free oligosaccharides in the cytosol. *Biochem. J.* **400,** 33–41

10. Saint-Pol, A., Codogno, P., and Moore, S. E. (1999) Cytosol-to-lysosome transport of free polymannose-type oligosaccharides. Kinetic and specificity studies using rat liver lysosomes. *J. Biol. Chem.* **274,** 13547–13555

11. Saint-Pol, A., Bauvy, C., Codogno, P., and Moore, S. E. (1997) Transfer of free polymannose-type oligosaccharides from the cytosol to lysosomes in cultured human hepatocellular carcinoma HepG2 cells. *J. Cell Biol.* **136,** 45–59

12. Chantret, I., and Moore, S. E. (2008) Free oligosaccharide regulation during mammalian protein *N*-glycosylation. *Glycobiology* **18,** 210–224

13. Anumula, K. R., and Spiro, R. G. (1983) Release of glucose-containing polymannose oligosaccharides during glycoprotein biosynthesis. Studies with thyroid microsomal enzymes and slices. *J. Biol. Chem.* **258,** 15274–15282

14. Shoup, V. A., and Touster, O. (1976) Purification and characterization of the α-ᴅ-mannosidase of rat liver cytosol. *J. Biol. Chem.* **251,** 3845–3852

15. Kuokkanen, E., Smith, W., Mäkinen, M., Tuominen, H., Puhka, M., Jokitalo, E., Duvet, S., Berg, T., and Heikinheimo, P. (2007) Characterization and subcellular localization of human neutral class II α-mannosidase (corrected). *Glycobiology* **17,** 1084–1093

16. Yanagida, K., Natsuka, S., and Hase, S. (2006) Structural diversity of cytosolic free oligosaccharides in the human hepatoma cell line, HepG2. *Glycobiology* **16,** 294–304

17. Costanzi, E., Balducci, C., Cacan, R., Duvet, S., Orlacchio, A., and Beccari, T. (2006) Cloning and expression of mouse cytosolic α-mannosidase (Man2c1). *Biochim. Biophys. Acta* **1760,** 1580–1586

18. Bernon, C., Carré, Y., Kuokkanen, E., Slomianny, M. C., Mir, A. M., Krzewinski, F., Cacan, R., Heikinheimo, P., Morelle, W., Michalski, J. C., Foulquier, F., and Duvet, S. (2011) Overexpression of Man2C1 leads to protein underglycosylation and up-regulation of endoplasmic reticulum-associated degradation pathway. *Glycobiology* **21,** 363–375

19. He, L., Fan, C., Kapoor, A., Ingram, A. J., Rybak, A. P., Austin, R. C., Dickhout, J., Cutz, J. C., Scholey, J., and Tang, D. (2011) α-Mannosidase 2C1 attenuates PTEN function in prostate cancer cells. *Nat. Commun.* **2,** 307

20. Tian, Y., Ju, J. Y., Zhou, Y. Q., Liu, Y., and Zhu, L. P. (2008) Inhibition of α-mannosidase Man2c1 gene expression suppresses growth of esophageal carcinoma cells through mitotic arrest and apoptosis. *Cancer Sci.* **99,** 2428–2434

21. Xiang, Z. G., Jiang, D. D., Liu, Y., Zhang, L. F., and Zhu, L. P. (2010) hMan2c1 transgene promotes tumor progress in mice. *Transgenic Res.* **19,** 67–75

22. Magin, T. M., McWhir, J., and Melton, D. W. (1992) A new mouse embryonic stem cell line with good germ line contribution and gene targeting frequency. *Nucleic Acids Res.* **20,** 3795–3796

23. Bradford, M. M. (1976) A rapid and sensitive method for the quantitation of microgram quantities of protein utilizing the principle of protein-dye binding. *Anal. Biochem.* **72,** 248–254

24. Hartmann, D., De Strooper, B., and Saftig, P. (1999) Presenilin-1 deficiency leads to loss of Cajal-Retzius neurons and cortical dysplasia similar to human type 2 lissencephaly. *Curr. Biol.* **9,** 719–727

25. Hennigar, R. A., Mayfield, R. K., Harvey, J. N., Ge, Z. H., and Sens, D. A. (1987) Lectin detection of renal glycogen in rats with short-term streptozotocin-diabetes. *Diabetologia* **30,** 804–811

26. Kmiécik, D., Herman, V., Stroop, C. J., Michalski, J. C., Mir, A. M., Labiau, O., Verbert, A., and Cacan, R. (1995) Catabolism of glycan moieties of lipid intermediates leads to a single Man5GlcNAc oligosaccharide isomer. A study with permeabilized CHO cells. *Glycobiology* **5,** 483–494

27. Morelle, W., Faid, V., Chirat, F., and Michalski, J. C. (2009) Analysis of *N*- and *O*-linked glycans from glycoproteins using MALDI-TOF mass spectrometry. *Methods Mol. Biol.* **534,** 5–21

28. Kukushkin, N. V., Alonzi, D. S., Dwek, R. A., and Butters, T. D. (2011) Demonstration that endoplasmic reticulum-associated degradation of glycoproteins can occur downstream of processing by endomannosidase. *Biochem. J.* **438,** 133–142

29. Mithieux, G. (2001) New data and concepts on glutamine and glucose metabolism in the gut. *Curr. Opin. Clin. Nutr. Metab. Care* **4,** 267–271

30. Kimura, K., Yamada, T., Matsumoto, M., Kido, Y., Hosooka, T., Asahara, S., Matsuda, T., Ota, T., Watanabe, H., Sai, Y., Miyamoto, K., Kaneko, S., Kasuga, M., and Inoue, H. (2012) Endoplasmic reticulum stress inhibits STAT3-dependent suppression of hepatic gluconeogenesis via dephosphorylation and deacetylation. *Diabetes* **61,** 61–73

31. Wang, Y., Vera, L., Fischer, W. H., and Montminy, M. (2009) The CREB coactivator CRTC2 links hepatic ER stress and fasting gluconeogenesis. *Nature* **460,** 534–537

32. Seo, H. Y., Kim, M. K., Min, A. K., Kim, H. S., Ryu, S. Y., Kim, N. K., Lee, K. M., Kim, H. J., Choi, H. S., Lee, K. U., Park, K. G., and Lee, I. K. (2010) Endoplasmic reticulum stress-induced activation of activating transcription factor 6 decreases cAMP-stimulated hepatic gluconeogenesis via inhibition of CREB. *Endocrinology* **151,** 561–568

33. Ashktorab, H., Green, W., Finzi, G., Sessa, F., Nouraie, M., Lee, E. L., Morgano, A., Moschetta, A., Cattaneo, M., Mariani-Costantini, R., Brim, H., and Biunno, I. (2012) SEL1L, an UPR response protein, a potential marker of colonic cell transformation. *Dig. Dis. Sci.* **57,** 905–912

34. Aranda-Abreu, G. E., Hernández, M. E., Soto, A., and Manzo, J. (2005) Possible cis-acting signal that could be involved in the localization of different mRNAs in neuronal axons. *Theor. Biol. Med. Model* **2,** 33

35. Barateiro, A., Vaz, A. R., Silva, S. L., Fernandes, A., and Brites, D. (2012) ER stress, mitochondrial dysfunction and calpain/JNK activation are involved in oligodendrocyte precursor cell death by unconjugated bilirubin. *Neuromolecular Med.* **14,** 285–302

36. Makioka, K., Yamazaki, T., Fujita, Y., Takatama, M., Nakazato, Y., and Okamoto, K. (2010) Involvement of endoplasmic reticulum stress defined by activated unfolded protein response in multiple system atrophy. *J. Neurol. Sci.* **297,** 60–65

37. Van Sluijters, D. A., Van Woerkom, G. M., Aerts, J. M., and Meijer, A. J. (1999) Sphingomyelinase treatment of rat hepatocytes inhibits cell-swelling-stimulated glycogen synthesis by causing cell shrinkage. *Eur. J. Biochem.* **266,** 653–659

38. Gustafson, L. A., Jumelle-Laclau, M. N., van Woerkom, G. M., van Kuilenburg, A. B., and Meijer, A. J. (1997) Cell swelling and glycogen metabolism in hepatocytes from fasted rats. *Biochim. Biophys. Acta* **1318,** 184–190

39. Zhu, M., Lovell, K. L., Patterson, J. S., Saunders, T. L., Hughes, E. D., and Friderici, K. H. (2006) β-Mannosidosis mice: a model for the human lysosomal storage disease. *Hum. Mol. Genet.* **15,** 493–500

40. Stinchi, S., Lüllmann-Rauch, R., Hartmann, D., Coenen, R., Beccari, T., Orlacchio, A., von Figura, K., and Saftig, P. (1999) Targeted disruption of the lysosomal α-mannosidase gene results in mice resembling a mild form of human α-mannosidosis. *Hum. Mol. Genet.* **8,** 1365–1372

41. Yue, W., Jin, Y. L., Shi, G. X., Liu, Y., Gao, Y., Zhao, F. T., and Zhu, L. P. (2004) Suppression of 6A8 α-mannosidase gene expression reduced the potentiality of growth and metastasis of human nasopharyngeal carcinoma. *Int. J. Cancer* **108,** 189–195

42. Wang, L., and Suzuki, T. (2013) Dual functions for cytosolic α-mannosidase (Man2C1). Its down-regulation causes mitochondria-dependent apoptosis independently of its α-mannosidase activity. *J. Biol. Chem.* **288,** 11887–11896